Dynamical effects induced by long range activation in a nonequilibrium reaction-diffusion system

M. Fuentes and M. N. Kuperman*
Centro Atomico Bariloche and Instituto Balseiro, 8400 San Carlos de Bariloche, Argentina

J. Boissonade,† E. Dulos,‡ F. Gauffre,§ and P. De Kepper‖
Centre de Recherche Paul Pascal (CNRS), avenue Schweitzer, F-33600 Pessac, France
(Received 17 July 2002; published 22 November 2002)

We show both experimentally and numerically that the time scales separation introduced by long range activation can induce oscillations and excitability in nonequilibrium reaction-diffusion systems that would otherwise only exhibit bistability. Namely, we show that in the chlorite-tetrathionate reaction, where the autocatalytic species H^+ diffuses faster than the substrates, the spatial bistability domain in the nonequilibrium phase diagram is extended with oscillatory and excitability domains. A simple model and a more realistic model qualitatively account for the observed dynamical behavior. The latter model provides quantitative agreement with the experiments.

DOI: 10.1103/PhysRevE.66.056205 PACS number(s): 82.40.Ck, 82.40.Bj

I. INTRODUCTION

Dynamics of spatial and spatiotemporal reaction-diffusion patterns in chemical systems kept far from equilibrium by a permanent feed of fresh reactants is an active domain of nonlinear science [1–3]. These patterns include traveling waves in oscillating or excitable media, Turing patterns, self-replicating spots, labyrinthine patterns, and dynamically structured fronts. They result from the destabilization of a trivial state of high symmetry by a positive feedback (''activation''), caused by autocatalysis or substrate inhibition, competing with a negative feedback on appropriate time scales. Although some patterns are transiently observed in some systems, these dissipative structures can only be sustained in permanently fed open reactors. Among these, the one-side-fed-reactor (OSFR) made of a thin slab of a chemically inert gel fed on one face and described further on in detail has become popular. Recently, a new type of dynamical behavior, namely, spatial bistability has been evidenced in this type of reactor [4].

Till now, two classes of spatial patterns have effectively been observed. In the first class, the primary source of the patterns is the dynamical properties of the reaction in homogeneous conditions. Reactions which oscillate or are excitable in homogeneous conditions, i.e. in well stirred reactors, give rise to traveling waves in unstirred media. The role of diffusion is to convert the temporal dynamics into spatiotemporal dynamics [5]. The phenomenon may occur whatever are the relative values of the diffusion coefficients of the different species. In the second class, the source of patterns is the so-called ''long range inhibition.'' An activatory species, i.e., a species which controls the positive feedback, like an autocatalytic species, diffuses much slower than the inhibitory species. This favors the growth of the instability at localized positions by creating two different time scales for spatial interactions [6]. The prototypes of such patterns are the stationary Tring patterns [7–9], but long range inhibition is also involved in other phenomena such as self-replicating spots [10], labyrinthine patterns [11], or morphological instabilities of fronts [12–14]. Since all small molecules in solution have almost the same diffusion coefficients, it was necessary to slow down the effective diffusion of the activatory species by complexation with immobile sites to meet these conditions experimentally [15,16].

Actually, ''long range activation'' where an activating species diffuses faster than an inhibitory species defines a third class of systems with several diffusive time scales. Like with long range inhibition, one expects this differential diffusion be responsible for new instabilities that are not present in the sole chemical kinetics. However, rather than inducing the growth of the perturbations more or less locally, the fast diffusing activator tends to excite perturbations at large distance from the initial inhomogeneities and to transform a stationary state into an excitable or an oscillatory one. In a recent study of spatial bistability in the chlorite-tetrathionate reaction, which exhibits long range activation, we have reported a preliminary observation of such a behavior [17]. Here, we report more extensive experimental data and detailed numerical studies of these phenomena.

In Sec. II we summarize former basic results on spatial bistability in OSFRs, and present the reaction, the models and the experimental systems. In Sec. III we report the results obtained with a simplified model to illustrate the general ideas. In Sec. IV part, we report both experimental results and numerical simulations with a more complete model. The Sec. V is devoted to the discussion of the results.

II. THEORETICAL AND EXPERIMENTAL MATERIALS

A. Spatial bistability

An OSFR is made of a film of a chemically resistant gel, of uniform thickness l. One face is kept in contact with the homogeneous contents of a continuous stirred tank reactor

*Electronic address: kuperman@cab.cnea.gov.ar
†Electronic address: boisson@crpp.u-bordeaux.fr
‡Electronic address: dulos@crpp.u-bordeaux.fr
§Electronic address: gauffre@crpp.u-bordeaux.fr
‖Electronic address: dekepper@crpp.u-bordeaux.fr

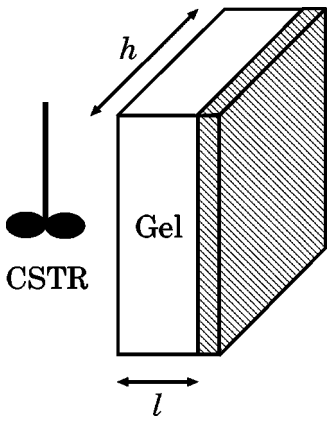

FIG. 1. Scheme of an OSFR.

(CSTR). The other face is pressed against an impermeable wall (Fig. 1). The coupled dynamical equations for the concentrations in the CSTR and in the gel are, respectively [4],

$$\frac{\partial c_{i\mathrm{h}}}{\partial t} = f_i(\mathbf{c}_\mathrm{h}) + \frac{(c_{i0} - c_{i\mathrm{h}})}{\tau} + \rho_V \frac{D_i}{l}\left(\frac{\partial c_i}{\partial r}\right)_{r=0}, \qquad (1)$$

and

$$\frac{\partial c_i}{\partial t} = f_i(\mathbf{c}) + D_i \nabla^2 c_i, \qquad (2)$$

where c_{i0}, $c_{i\mathrm{h}}$, and c_i are the concentrations of species i, respectively, in the input flow, in the CSTR, and inside the gel, D_i is the corresponding diffusion coefficient, τ is the residence time of the reactor , ρ_V is the ratio of the volume of the gel to the volume of the CSTR, and r is the distance to the CSTR-gel interface. The f_i's are the reaction rates. In the right hand side of Eq. (1), the three terms represent the change of the concentrations per time unit. The first term gives the contribution of the reaction. The second one represents the input and output flows of the species. It contains all the expandable control parameters of the system, namely, τ and the c_{i0}. The third term results from the diffusive flux of the species at the interface between the gel and the CSTR and represents the feedback of the gel contents on the CSTR dynamics. When the volume of the CSTR is large in regard to the volume of the gel ($\rho_V \ll 1$), this last term can generally be dropped so that the chemical state of the CSTR is independent of the state of the gel and the concentrations in the CSTR define a Dirichlet boundary condition for Eq. (2) at $r=0$, whereas a no-flux boundary condition is applied at $r=l$. To avoid ambiguities, let us make more precise the terms we use. Whereas in usual OSFRs the thickness l is small in regard to the two other dimensions, in this paper, we want to investigate the behavior of the system along the direction orthogonal to the faces in contact with the CSTR and the impermeable wall. Thus, we shall consider systems made of ''flat'' gels in which one of the dimensions parallel to these faces (h in Fig. 1) is still smaller and negligible. Such systems can be considered as two dimensional. Nevertheless, the size l, in the direction orthogonal to the faces, remains small in regard to the second direction parallel to these faces. Size l and the direction orthogonal to the faces will be further referred to as the ''depth'' or the ''width'' of the gel, the negligible dimension h becoming the ''thickness.''

A number of reactions which present autocatalytic steps are bistable in a CSTR [1,3,18]. These reactions normally exhibit ''clock'' behavior in batch conditions, i.e., a more or less long induction period followed by a fast switch to the equilibrium. In these reactions, the transformation rate of the substrate(s) tremendously increases during the switch which occurs when the level of the autocatalytic species is large enough. For residence times much shorter than the typical reaction time, i.e., at high flow rates, the composition inside the CSTR is close to the composition in the input flow. It is referred as the ''flow state'' or state F. For residence times much larger than the typical reaction time, i.e., at low flow rates, the reaction is almost completed in the CSTR and the composition in the CSTR is close to a thermodynamic equilibrium. This is referred as the ''thermodynamic state'' or state T. For intermediate flow rates, both states are stable for the same composition of the input flows. Spatial bistability can be observed when such a reaction is operated in an OSFR, the CSTR of which is set in the flow state. Although this phenomenon, which extends the concept of bistability to space, has been previously described in simple models [18] and in real experiments [19,20], its importance has been recognized only recently, and a detailed analysis was worked out in relation with the development of the OSFRs [4,21,22].

To understand the basic principles of spatial bistability, let us consider the concentration profile of a substrate of concentration X and diffusion coefficient D consumed in the reaction and let us imagine that the depth l of the gel can be changed in a continuous way. The time taken by fresh reactants fed by diffusion at the CSTR boundary to reach the opposite boundary is of the order of $t_D = l^2/D$. We start from $l=0$ and increase l adiabatically so that the system is always in its asymptotic stationary state. Let t_i be the induction time for the CSTR composition (in state F). While l is small enough for $t_D \ll t_i$ to hold, the whole volume of the gel remains in state F. We shall still refer this state of the gel as a F state. When t_D reaches a value of the order of t_i, for a value $l = l_{\max}$, the fast reaction starts at the impermeable wall and a steep front connecting the F state to a T state forms. Such a state will be referred as a ''mixed state'' or FT state. But, the amount of the autocatalytic species is now large at the impermeable wall of the gel ($r=l$) and can diffuse backwards switching on the reaction, so that the front can recede to a value $l = \delta < l_{\max}$. Actually, if one assumes that the reaction rate is extremely large inside the front, one can neglect the rate of the consumption of the substrate elsewhere and the concentration of the latter can be approximated by the solution of a diffusion equation between a fixed value at $r=0$ (the CSTR) and $r=\delta$ (the front). Then, it can easily be shown that

$$\delta \approx \frac{D_i |\Delta X| S}{\dot{Q}}, \qquad (3)$$

where $\dot{Q}$ is the total amount of substrate converted by time unit in the gel, ΔX is the variation of concentration between

the F and the T states and S is the surface of the film [4]. This value is practically independent of l, so that one can now decrease l down to a value $l_{\min} \sim \delta$ before the system switches back from the FT to the F state. Thus, for $l_{\min} < l < l_{\max}$, both concentrations profile F and FT are stable. This defines the spatial bistability. The extent of the bistability domain depends on the concentrations in the CSTR—always close to those in the input flow—and the residence time, so that various nonequilibrium phase diagrams can be built [4,17,22]. In spite of its apparent crudeness, this theory gives accurate results. Extensive studies have been performed experimentally and numerically on the chlorine dioxide-iodide (CDI) reaction. Till now, differences in diffusion coefficients did not seem to play any role. Actually, whether the system is ruled by equal diffusion coefficients or by long range inhibition, it exhibits a standard spatial bistability. We shall see that the situation is fairly more complex when long range activation comes into play.

B. The chlorite-tetrathionate reaction

The chlorite-tetrathionate (C-T) reaction has essentially been studied in closed systems for the determination of stoichiometric and kinetic aspects [23,24] as well as a source for propagating cellular fronts [12–14]. In excess of chlorite, the reaction kinetics is well approximated by the following overall balance equation:

$$7\mathrm{ClO_2^-} + 2\mathrm{S_4O_6^{2-}} + 6\mathrm{H_2O} \rightarrow 7\mathrm{Cl^-} + 8\mathrm{SO_4^{2-}} + 12\mathrm{H^+}, \quad (4)$$

and the reaction rate by

$$v_R = -\frac{1}{7}\frac{d[\mathrm{ClO_2^-}]}{dt} = k[\mathrm{ClO_2^-}][\mathrm{S_4O_6^{2-}}][\mathrm{H^+}]^2. \quad (5)$$

Since, during the reaction, large pH changes are observed, the fast dissociation equilibria of H_2O and HSO_4^- also have to be accounted for. This rate law exhibits quadratic autocatalysis in $[H^+]$. Although the validity of this rate law has been determined for a limited range of pH (4.7–5.5) [23], it has been successfully used in much larger domains. Nevertheless, the original value $k = 10^9\ \mathrm{M^{-3}\,s^{-1}}$ had to be adjusted to fit with experiments. The value $k = 5 \times 10^6\ \mathrm{M^{-3}\,s^{-1}}$ has recently been proposed to fit the experimental data of the bistability domain of the reaction in a CSTR [17] and will be used in the following.

It is well known that, whereas most species have a diffusion coefficient close to $10^{-5}\ \mathrm{cm^2\,s^{-1}}$, the autodiffusion coefficient of the proton H^+ is almost ten times larger. Nevertheless, accounting for the electroneutrality condition and the presence of the slowest ions, the effective diffusion of H^+ is lower [25]. Solving reaction-diffusion equations that include all ionic effects is a formidable task which has been only performed on simple models [26]. For practical reasons, it is reasonable to use a constant and uniform effective value for each diffusion coefficient. We shall assume that all diffusion coefficients are equal to a unique effective value D_1, except for H^+ and OH^- which have both a higher autodiffusion coefficient and are closely related. Let D_2 be a common value for these two species. With these assumptions, it was shown in Ref. [17] that the experimental data can be correctly interpreted only if $d = D_2/D_1$ ranges slightly above three. Thus it is necessary to take into account that the autocatalytic species H^+ diffuses much faster than the inhibitory species, so that the reaction-diffusion system enters the class of long range activation.

C. The simple model

In order to make extensive computations, we shall first define a simple model, the properties of which are close enough to the original system to draw significant conclusions. Our main purpose is that, due to its formal simplicity, this model can be further used as a prototype for long range activation. The model relies on two strong assumptions: The kinetics is completely described by Eqs. (4) and (5), and the concentrations at the CSTR boundary are fixed to their values in the input flow, i.e., we assume a residence time $\tau = 0$ (infinite flow rate). In these conditions, the reaction-diffusion system is

$$\frac{\partial[\mathrm{ClO_2^-}]}{\partial t} = -7k[\mathrm{ClO_2^-}][\mathrm{S_4O_6^{2-}}][\mathrm{H^+}]^2 + D_1\nabla^2[\mathrm{ClO_2^-}], \quad (6)$$

$$\frac{\partial[\mathrm{S_4O_6^{2-}}]}{\partial t} = -2k[\mathrm{ClO_2^-}][\mathrm{S_4O_6^{2-}}][\mathrm{H^+}]^2 + D_1\nabla^2[\mathrm{S_4O_6^{2-}}],$$

$$\frac{\partial[\mathrm{H^+}]}{\partial t} = 12k[\mathrm{ClO_2^-}][\mathrm{S_4O_6^{2-}}][\mathrm{H^+}]^2 + D_2\nabla^2[\mathrm{H^+}].$$

In this paper, we do not consider short transients that follow a change of parameters and only consider the asymptotic regime. Eliminating the reaction term between the first two equations, one is left with a diffusion equation with a fixed boundary condition at $r = 0$. In the long time limit, the solution is $2[\mathrm{ClO_2^-}] - 7[\mathrm{S_4O_6^{2-}}] = 2[\mathrm{ClO_2^-}]_0 - 7[\mathrm{S_4O_6^{2-}}]_0$, where index 0 holds for the concentrations fixed at the boundary. Then $[\mathrm{S_4O_6^{2-}}]$ can be expressed as a function of $[\mathrm{ClO_2^-}]$ and can be eliminated from Eqs. (6). One gets the two-variable reduced system

$$\frac{\partial u}{\partial t'} = -(u-\xi)uv^2 + \nabla_{r'}^2 u, \quad (7)$$

$$\frac{\partial v}{\partial t'} = \frac{12}{7}(u-\xi)uv^2 + d\nabla_{r'}^2 v,$$

where we have introduced the new time and space scales $t' = 2k([\mathrm{ClO_2^-}]_0)^3 t$, $r' = (2k/D_1)^{1/2}([\mathrm{ClO_2^-}]_0)^{3/2} r$ and the following normalized variables and parameters: $u = [\mathrm{ClO_2^-}]/[\mathrm{ClO_2^-}]_0$, $v = [\mathrm{H^+}]/[\mathrm{ClO_2^-}]_0$, $d = D_2/D_1$, and $\xi = 1 - (7/2)[\mathrm{S_4O_6^{2-}}]_0/[\mathrm{ClO_2^-}]_0$. This system is formerly identical to the system used in previous studies in closed systems [24]. According to the definition of u, one has $u = 1$ at the CSTR boundary. Thus, the control parameters are v_0, d, and ξ, where v_0 is the fixed value of v at the CSTR

boundary. Parameter ξ represents the normalized excess of chlorite. Provided it is not too large—this is the case in most experiments—it was found to play a minor role in the model and does not bring qualitative changes in the results. Thus, it was fixed at $\xi=0$ that would correspond to exact stoichiometric proportions of chorite and tetrathionate.

Note that, if $d=1$, the third equation could be eliminated in the same way and the system would be reduced to a unique variable u. A similar reduction to the same one-variable equation could also be done for a homogeneous CSTR. A one-variable system can be bistable but never oscillating or excitable, since two dynamical time scales at least are necessary. This suggests that the C-T reaction can be neither oscillating or excitable in a CSTR. More sophisticated models support this assertion, which is confirmed by experiments.

This model suffers from serious limitations. First, at the CSTR boundary, we use fixed concentrations equal to the concentrations in the input flow. Since, in the flow state, the concentrations should be close to those in the input flows, this seems to be a reasonable approximation. Nevertheless, at finite residence times, the values of v_0 could correspond to nonexistent or unstable states of the CSTR. The approximation is strictly valid only in the practically unreachable limit of infinite flow rates ($\tau=0$). In the same way, one can fix v_0 to arbitrarily high values for which the CSTR would necessarily be in a T state. This can lead to ambiguities in the definition of the spatial states F and T and to experimentally unreachable regions in phase diagrams so that some care is necessary for their interpretations. Finally, values of v_0 can also be taken arbitrarily low, down to zero, an unrealistic situation since the dissociation equilibrium of water imposes that $[H^+]$ remains positive and finite. Thus, this model must be only thought as a ''toy model,'' with the advantage that the kinetics remains closely related to that of a real system. This will allow us to evidence dynamical phenomena induced by long range activation. Such models have also been recently used by Benyaich *et al.* in studies of spatial bistability [27]. To make direct comparison with experiments, a more elaborated model has to be devised.

D. The extended model

To avoid oddities due to the simple model oversimplifications, one has to account, not only for the dynamics of the CSTR at $r=0$ included in the Eq. (1), but also for the way in which the H^+ ions are introduced in the reactor and the equilibria in which they are involved. In the extended model that we used to make comparisons with the experimental results, the following fast equilibria are taken into account in addition to Eq. (4):

$$H^+ + OH^- \rightleftharpoons H_2O, \tag{8}$$

with rate law

$$v_e = k_e^+ - k_e^-[H^+][OH^-], \tag{9}$$

and

$$H^+ + SO_4^{2-} \rightleftharpoons HSO_4^-, \tag{10}$$

with rate law

$$v_a = k_a^+[HSO_4^-] - k_a^-[H^+][SO_4^{2-}]. \tag{11}$$

Discarding the species that do not contribute to kinetics in Eqs. (4), (8), and (10), one retains the six variables $[H^+]$, $[OH^-]$, $[ClO_2^-]$, $[S_4O_6^{2-}]$, $[SO_4^{2-}]$, and $[HSO_4^-]$. The following values are used for the kinetic constants [28,29]: $k_e^- = 1.4\times10^{11}\ \mathrm{M\,s^{-1}}$, $k_e^+ = K_e k_e^-$ with $K_e = 10^{-14}$, $k_a^- = 10^{11}\ \mathrm{M\,s^{-1}}$, $k_a^+ = K_a k_a^-$ with $p\mathrm{K}_a = -\log_{10}(K_a) = 1.94$. The diffusion coefficient D_1 is fixed at a standard value $D_1 = 10^{-5}\ \mathrm{cm^2\,s^{-1}}$ and the fast species diffusion coefficient D_2 is fixed at $D_2 = 3.4\times10^{-5}\ \mathrm{cm^2\,s^{-1}}$ to fit at best the experimental data. Accurate one-dimensional numerical solutions of the resulting reaction-diffusion system have been obtained by an implicitly finite difference method for stiff systems with adaptative grid in time and space by the method of lines with a second-order spatial scheme. The time integrator is a fourth-order Rosenbrock method [30] or the semi-implicit Bader-Deuflhard method [31]. Unfortunately, due to the higher complexity and the extreme stiffness of the model, it was impossible to make systematic studies of this model in higher dimensions. Two-dimensional computations were limited to a few points in parameter space. In order to avoid problems in the definition of the input concentrations and to make easier the comparisons with the experimental data and a previous work, we use, as the main control parameter, the quantity α defined in the experimental section below.

E. Experimental conditions

In order to resolve the concentration profiles in the depth l of the reactor and to minimize both technical difficulties and parasitic edge effects, we have developed one-side-fed flat annular reactors, i.e., annular OSFRs. Complete descriptions and technical details on such reactors can be found in Ref. [4]. These OSFRs are made of a flat annular piece of 2% agarose gel, of thickness $h \leqslant 0.5$ mm. They have a fixed outer radius $R_{\mathrm{out}} = 12.5$ mm and an inner radius R_{in} such that the width $l = R_{\mathrm{out}} - R_{\mathrm{in}}$ ranges from 0.5 to 3 mm. The agarose gel can be considered as chemically inert in regard to the reaction. In this soft hydrogel, the diffusion coefficients are close to those in pure water. The ratio R_{in}/l is large enough for the curvature effects to be negligible. The inner rim of the annulus is tighten against the impermeable boundary while the outer rim is in contact with the contents of a CSTR of 25 $\mathrm{cm^3}$, fed through a single inlet port with appropriately premixed solutions of reagents stored in separated reservoirs. The residence time of the reactor $\tau = 600$ s, the temperature $T = 25°\mathrm{C}$, and the input flow concentrations of sodium chlorite $[NaClO_2]_0 = 1.9\times10^{-2}\mathrm{M}$ and potassium tetrathionate $[K_2S_4O_6]_0 = 0.5\times10^{-2}\mathrm{M}$ are kept fixed during all the experiments. All the solutions were made from reagent-grade chemicals in high quality deionized water. Besides the two above mentioned reagents, variable mixtures of perchloric acid and sodium hydroxide are added to the input flow of reagents to control the pH of the premixed feed solution.

This is done by pumping different volume ratios of acid and base, keeping the overall flow rate constant. For experimental and graphic convenience, this relative distribution is characterized by a control parameter α on which the acid and base flow concentrations depend linearly: one has $[HClO_4]_0=\alpha\times 0.67\ 10^{-2}$M and $[NaOH]_0=(1-\alpha)\times 3.33\ 10^{-2}$M. The pH of the feed mixture decreases from a basic to an acid state as α increases from 0 to 1. The parameter α effectively controls the pH of the solution and is the only expandable control parameter in this series of experiments. The patterns are made visible by bromophenol blue (1% solution), a pH sensitive indicator that turns from dark purple in the basic state to pale yellow in the acid state. Patterns are monitored by a CCD camera connected to a time lapse video recorder.

The dynamics of the C-T reaction operated in the CSTR exhibits bistability in the range $0.18<\alpha<0.84$ between a F branch (with pH values typically above nine) and a T branch (with pH values typically below three). The upper limit corresponds to the value of α where the input flow switches from a basic to an acid solution. The lower limit was used to adjust the rate constant k to the value $k=5\times 10^6 \mathrm{M}^{-3}\,\mathrm{s}^{-1}$ [17].

III. THE SIMPLE MODEL ANALYSIS

In the preliminary experiments of Ref. [17], we had observed, in addition to spatial bistability, oscillations of the FT state front and excitability phenomena in the domain where the sole F state is stable. While the stability of concentration profiles can be determined with 1D simulations, the latter needs 2D computations. Thus, the stability limits are determined in 1D calculations by the same accurate implicit method as the full model and the existence of excitability domain is studied in two-dimensional simulations, performed with two different numerical methods. The first one is an implicit finite difference hopscotch method [32,33] with automatic step control added. The second one is a standard finite element method, with a Crank-Nicholson scheme. The mesh was composed by triangular elements. Neither perturbations nor fluctuations were added but the initial one and the inhomogeneities corresponding to numerical noise due to the implicit irregularity of the triangular mesh.

First, choosing a typical depth value $l=10$ (expressed in reduced units precedently defined), we have built a stability diagram in the plane $(v_0,d>1)$ (Fig. 2). At low values of v_0 and d, there is a large region of spatial bistability that extends down to $v_0=0$. When $v_0\to 0$ the acid state must obviously be obtained by a continuous decrease of v_0 from another acid state or by an acid perturbation of the system. In Fig. 3, are shown the two stable concentration profiles through the depth of the gel for a given set of control parameters. Contrary to the standard case, in the FT state, these profiles are always monotonous and do not exhibit a steep front. The states are nevertheless well characterized by the low (basic) or high (acid) value of v at $r=l$, the impermeable boundary of the gel. When $d\gg 1$, the system exhibits temporal oscillations in place of bistability. Since the system cannot oscillate in homogeneous conditions, these oscillations clearly result from the different time scales introduced by the differential diffusion. Although the problem is of spatial nature, the stability limits present the characteristic topology of the so-called ''cross-shaped diagram'' that connects bistability and oscillations of numerous reactions in homogeneous conditions [34].

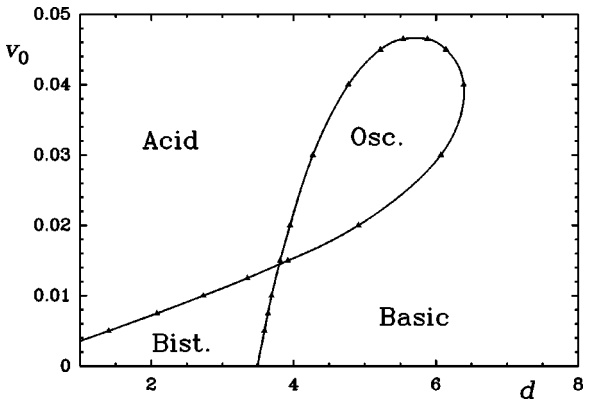

FIG. 2. Nonequilibrium phase diagram of the simple model at $l=10$ in the plane (d,v_0).

A second diagram in the plane (v_0,l) has been extensively computed for $d=5.5$, a value chosen for the richness of the dynamical situations exhibited at this diffusion ratio (Fig. 4). For small depths, the system is always in the flow (or basic) state, as expected. At intermediate values of depth, there is a large domain of oscillations. It vanishes at large v_0 values for which one continuously changes from the basic to the acid state when l is increased. For large depths, the FT (or acid) state is again present down to $v_0=0$, which defines a domain of spatial bistability at small v_0 values. The most interesting part of this diagram is the region labeled Bist. 2 in Fig. 4(b). In this narrow region, the system still exhibits spatial bistability, but the acid state becomes oscillating. Thus, the bistability domain is divided into two regions, one of standard bistability between two stationary concentration profiles (Bist. 1), and a second one between a stationary profile and an oscillating one (Bist. 2). Moreover, when one decreases l and crosses the stability limit of the oscillatory acid state, the unique stable state, namely, the F (basic) state,

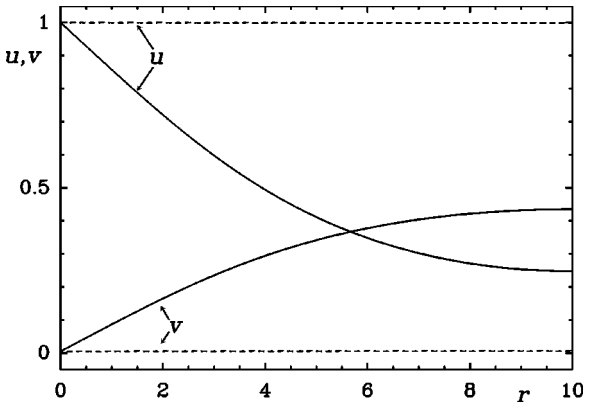

FIG. 3. Spatial bistability in the simple model: profiles of u and v as a function of depth. Dotted lines, F state ; full lines, FT state. Parameters, $l=10$, $d=3$, and $v_0=0.005$.

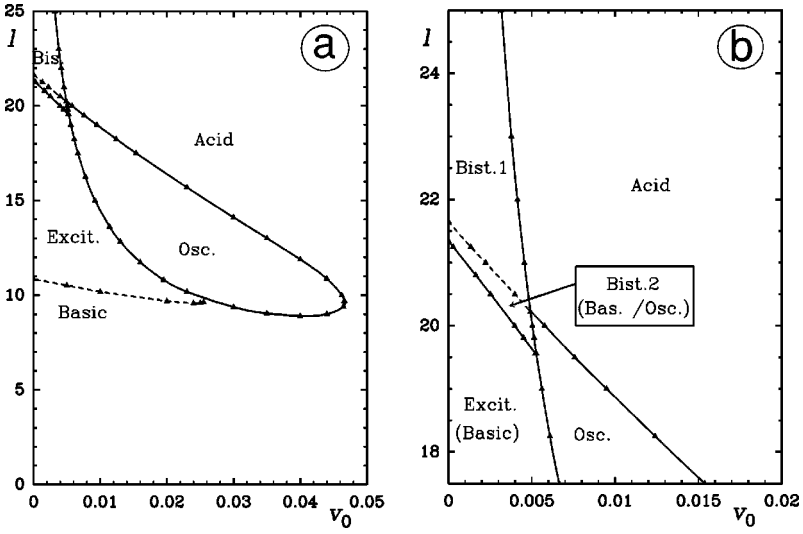

FIG. 4. Nonequilibrium phase diagram of the simple model at $d=5.5$ in the plane (v_0,l). (a) Large view. (b) detail of (a).

exhibits particular properties. If, in this stable state, an acid perturbation (such as $v=1$) is applied close to the impermeable wall, the perturbation does not smoothly decay to the stable state but stimulates a further increase of H^+ ions concentration in its vicinity. A pair of pulses forms and propagates along the wall in opposite directions. After relaxation of transients, they travel with constant shape, amplitude, and velocity, which precisely defines the phenomenom of excitability. The limits of this excitability domain are reported in Fig. 4(a). This domain extends all the way to the oscillation zone. In the vicinity of this latter zone, the recovery tail of the pulse can become oscillatory in space. Although, for more efficiency, these limits have been accurately computed in a rectangular reactor, we have also performed some runs in an annulus, analog to that of the experimental device. An example of an excitation pulse propagating in such an annulus (partial view) is represented in Fig. 5. The limits of this excitability domain are reported in Fig. 4(a). This domain extends to the oscillation zone. In the vicinity of this latter zone, the recovery tail of the pulse can become oscillatory in space.

IV. EXTENDED MODEL ANALYSIS AND EXPERIMENTAL RESULTS

In this section, we report the numerical results that have been obtained with the extended model and simultaneously make a direct comparison with the experimental data. We consider the existence and stability of the *F* state and the *FT* state in the plane (α,l).

Spatial bistability is observed over a significant domain of the plane. For instance, in Fig. 6, we show the two stable concentration profiles (*F* and *FT* states) computed for a same set of control parameter corresponding to a point located inside the bistability domain. Contrary to the case of the simple model, the *FT* state exhibits a steep front. The concentration profile of the autocatalytic species H^+ is plotted in logarithmic scale to emphasize on the position and the stiffness of the front. The concentration of $S_4O_6^{2-}$ and OH^- are represented in linear coordinates to underline the linear drop of the substrates concentrations as predicted by Eq. (3).

FIG. 5. Excitability in the simple model, traveling pulse. Concentration map of v, from minimum (black) to maximum (white). Parameters, $l=20$, $R_{ext}=150$, $d=5.5$, and $v_0=0.004$.

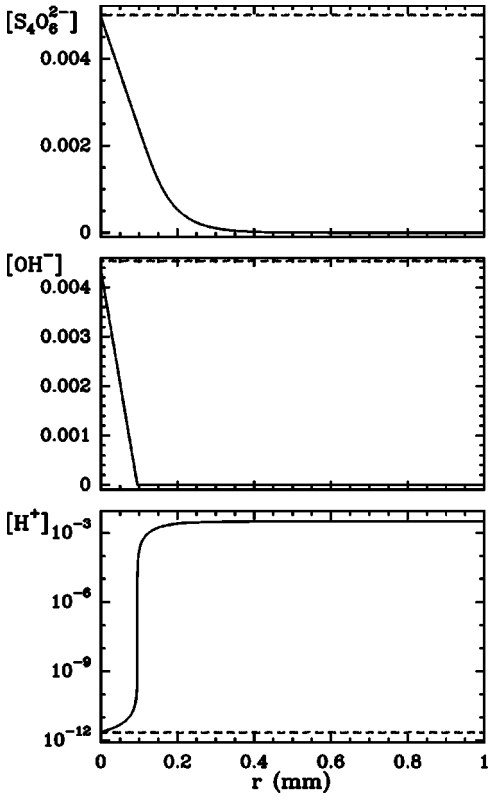

FIG. 6. Computed concentration profiles through the gel depth. All concentrations are in mol/l. Parameters, $l=1$ mm, $\alpha=0.72$. Dotted lines, *F* state; Full lines, *FT* state.

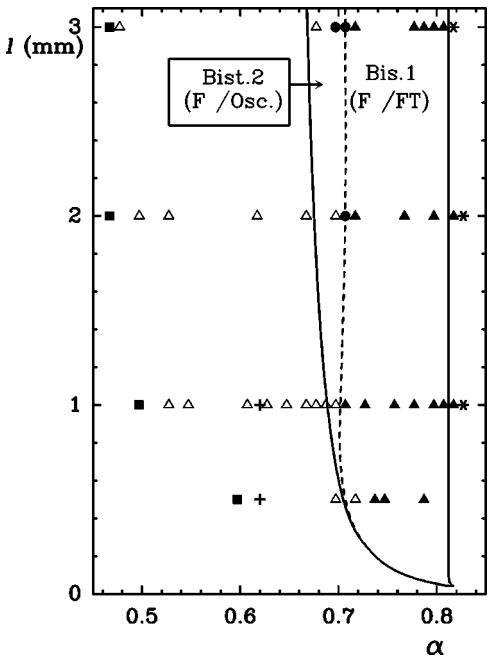

FIG. 7. Nonequilibrium phase diagram in the plane (α, l). Experimental points, ■ monostable with nonexcitable F state, △ monostable with excitable F state, ● bistable with oscillatory FT state, ▲ bistable with stationary FT state, * the CSTR switches to the thermodynamic state. Computed results, the full lines are the limits of the bistability domain, the dotted line is the limit of the oscillory FT state within the bistability region, + marks are points for which the F state has been shown to be excitable.

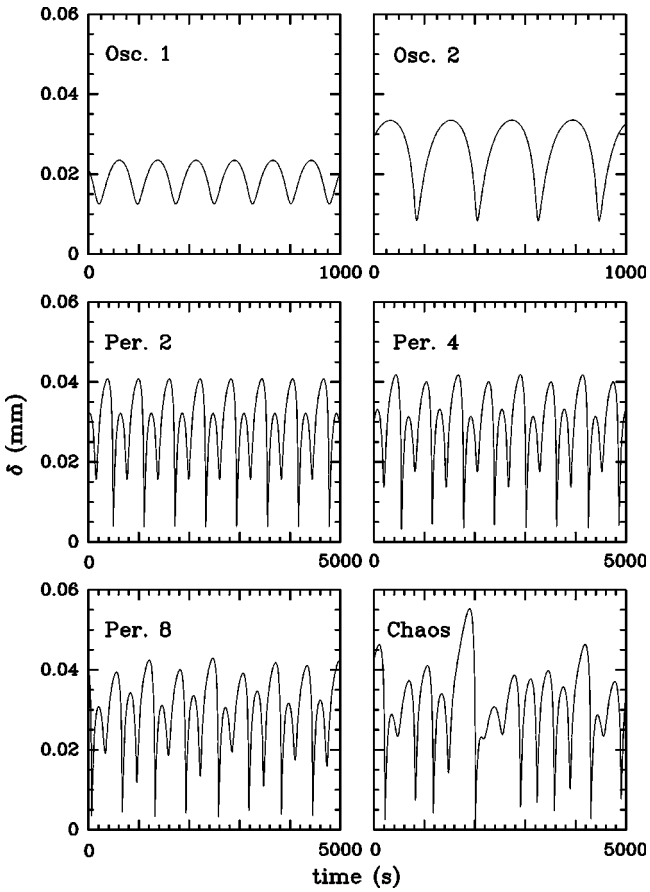

FIG. 8. Computed oscillations of the front position δ ($l=1$ mm), oscillation 1, $\alpha=0.700$; oscillation 2, $\alpha=0.692$; period 2, $\alpha=0.6895$; period 4, $\alpha=0.6894$; period 8, $\alpha=0.6892$; chaos: $\alpha=0.6885$.

In experiments, the pH color indicator reveals the two different states [17]. In the FT state, the gel is found to remain in a basic state only in a narrow band located along the outer rim. The nature of the different dynamical states was determined unambiguously in the whole parameter range that was explored.

In Fig. 7, we report the computed limits of the bistability domain (full lines) in the plane (α,l) and the experimental points. Gel annuli with $l<0.5$ mm could not be technically achieved, so that this part of the diagram cannot be explored experimentally. Numerically, the upper limit $\alpha_{\max}$ of the FT state is slightly lower than the limit $\alpha_T=0.833$ computed for the F state in the CSTR. Actually, in the FT state, the concentration gradients of the substrates at $r=0$ are large as seen in Fig. 6, so that, although $\rho_V \ll 1$, the last term in Eq. (1) is not completely negligible and the contents of the CSTR are entrained into the T state slightly before the limit $\alpha=\alpha_T$ is reached. Experimentally, this minor deviation is too small to be detected. There is a first major difference with the standard CDI reaction [4]: The spatial bistability persists at large values of l, which seems in contradiction with our theoretical presentation asserting that the F state cannot exist when the width of the gel is large. Actually, this results from the extreme slowness of the reaction when the system is in the basic F state. This leads to a quasi-infinite induction time. Thus, one cannot switch spontaneously from the F state to the FT state by a continuous change of l, if one remains within a realistic range. Nevertheless, one reaches this state by an appropriate perturbation or choice of the initial condition in the gel, but the bistability domain extends to huge values of the depth l.

Contrary to the standard case of the CDI reaction, the limit of the FT state when α decreases at constant l is complex and exhibits dynamical phenomena both numerically and experimentally, provided that l is large enough as seen in Fig. 7. When the value of α decreases and crosses the dotted line, the position of the front begins to oscillate and δ becomes a function of time. This domain of oscillatory dynamics is narrow and difficult to explore precisely in experiments. However, one-dimensional numerical simulations allow for a precise exploration of this oscillatory domain. In Fig. 8, we represent the numerical oscillations for decreasing values of α at $l=1$ mm, but similar sequences are observed for other widths of the gel. When α decreases, the amplitude of the oscillations increases and they take a more and more relaxation character. When the α values are drawn still closer to the stability of the FT state, one observes, over a very narrow range of α values, a period doubling sequence leading to chaotic oscillations. When α decreases from the onset of oscillations, the period of the oscillations slowly increases. On the contrary, the period strongly increases when the width l increases. Since the experimental conditions are never strictly uniform all along the outer rim of the gel and

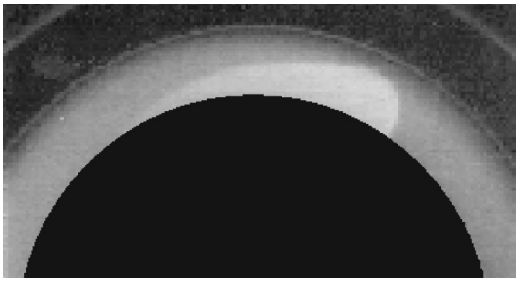

FIG. 9. Excitation pulse (experimental): an acid pulse (clear color) propagates to the right along the inner rim. $l=3$ mm, $\alpha=0.48$.

since the width l cannot be perfectly constant, the oscillations of the front lead to the formation of pacemakers that emit traveling waves with periods comparable to those found in the computations.

Beyond the stability limit of the FT front, dynamical phenomena persist in the form of excitability. In a large domain of parameters, an acid perturbation, made at a localized place of the gel annulus, propagates under the form of two opposite traveling pulses along the inner rim. After a short transient, each pulse takes a stationary shape and travels without deformation along the annulus (Fig. 9). The length of the pulse tail decreases as α decreases until the excitability is eventually lost. When the pulses meet, they anihilate each other, but by adding a basic perturbation at the right place and time, it is possible to anihilate one of the two pulses. Then, the surviving pulse can rotate indefinitely along the annulus as previously done with the Belousov-Zhabotinski reaction, the paradigm of excitable reactions [35,36]. This behavior is identical to that observed with the simple model and is also reproduced with the extended model for the two different sets of parameters that were checked for excitability.

V. DISCUSSION AND CONCLUSION

It is known that, in homogeneous bistable systems, the addition of a negative feedback that introduces a new time scale can induce oscillations. In the same way, excitability can arise from the coupling of a bistable subsystem that exhibits a *S*-shaped nulcline with the feedback dynamics of a recovery variable.

Our simple model has clearly shown that the additional time scales introduced by long range activation can play a similar role and are able to induce excitability and spatiotemporal oscillations in a system which can only be bistable in homogeneous conditions. When the diffusion of the activator is not significantly higher than the diffusion of the other species, the system can only exhibit spatial bistability. But, when the ratio d becomes significantly larger than 1, the system exhibits a domain of oscillations connected to the bistable region; the diagram has a typical cross-shaped topology [37]. In a narrow band within the bistability region, the acid state can also become oscillatory. This is an analog to the experimental observations and to the results produced by the extended model.

Moreover, an excitability region develops along the stability limit of the FT state. Actually, there is no discontinuity between a stable FT state and an excitable pulse with an infinite recovery tail within the F state. One must be aware that the recovery is not controlled by a slow kinetic process imbedded in the reaction mechanism as for the Belousov-Zhabotinskii reaction, but by the diffusion process that rules the feed from the CSTR boundary. Thus, the excitability properties do not only depend on intrinsic quantities, i.e., the reaction rates and diffusion coefficients, but also on a geometrical characteristic of the reactor, namely, the depth of the gel.

Nevertheless, although the simple model predicts that differential diffusion can induce oscillations of the FT state in the spatial bistability region and excitability of the F state, the global agreement with experimental data, as well as with the extended model, is not very good. Except for some analogies in the left upper part of Fig. 4, the shape of the diagrams is different. A first reason is that the regions located on the right side of the bistable and the basic domains, including the oscillation pocket, are not physically reachable. The corresponding values of v_0 could not be maintained in the CSTR with realistic residence times. The CSTR would switch into a thermodynamic state. By the way, with this model, it is difficult to speak of a true FT state since the concentration profiles do not exhibit any front. This is why we prefer to use the terms basic or acid rather than F and FT when speaking of the simple model. The second major reason is that OH^- and the autocatalytic species H^+ are related by a strong constraint independent of the C-T reaction itself, namely, the fast equilibrium of water dissociation. This leads to buffering processes and excludes that v_0 takes values close to zero, as permitted by the simple model. Thus this toy model, which allows for extensive numerical calculations, is an excellent tool to demonstrate the mechanisms of long range activation phenomena, but it should not be used for a precise analysis of the properties of the real system. In particular, it would be illusive to try to connect quantitatively the model parameters with realistic quantities.

In the extended model, where the CSTR dynamics is included, a direct comparison with experiments is possible. Spatial bistability limits are in good agreement. There is nevertheless a point that deserves special attention. Species $S_4O_6^{2-}$ and ClO_2^- are the natural substrates, but since the system is fed with a basic solution, OH^- must be considered as another substrate in spite of its special relation with H^+. Since the diffusion coefficients of these substrates are not equal, there is an ambiguity in the choice of the species to be considered in the basic theory that leads to Eq. (3). Figure 6 clearly shows that the relevant species is OH^-. Its concentration drops linearly down to very low values at the exact position of the front, whereas the other substrates do not exhibit a linear drop all the way down and their concentration is far from minimal at the position of the front. A natural explanation is that, although OH^- diffuses fast, H^+ reacts much faster with OH^- than with the other substrates. This defines the smallest δ value and controls the overall process. However, the tail of the concentration profiles of these other subtrates plays a role in the anticipation of the $FT \rightarrow F$ tran-

sition that is actually found in the computations.

Like in the simple model, oscillations induced by the long range activation are observed. If one decreases α within the bistability domain, the FT state becomes oscillatory when its stability limit is approached. The diagram is in good quantitative agreement with experimental observations. Since oscillations are restricted to a narrow region of control parameters, the unavoidable small inhomogeneities along the annulus make it impossible to perform a fine analysis of this front dynamics. In the model, the complex oscillations and the period doubling sequence observed in the 1-D simulations can be understood using the following arguments. Actually, coupled oscillators may present the same complex dynamical behavior. Close to the onset of the oscillatory regime, the motion of the front exhibits simple periodicity. The amplitude of the oscillations $\delta_{\max}-\delta_{\min}$ is small and the front remains located close to the CSTR boundary. But when α decreases, approaching the limits of existence of the FT state, this amplitude becomes larger and larger. When $\delta_{\max}$ is of the order of l, the impermeable wall acts as a reflector for the diffusive concentration fields. Then, the front dynamics couples with itself, with delay and partial damping. This dynamics of coupled oscillators explains the observed dynamical complexity.

In spatial bistability, it is possible to prepare two regions of the reactors in the two different states F and FT side by side and to study the dynamics of the F/FT interface. In the standard case, the direction of propagation of this interface depends on the control parameters and changes within the bistability domain according to the relative stability of the two states F and FT as was experimentally shown with the CDI reaction [21,4]. In the C-T reaction, this situation is radically different. Because the fast diffusion of the autocatalytic species excites the medium ahead of the interface, the FT state propagates always into the F state, i.e., within the whole domain of spatial bistability. Moreover, this behavior can persist beyond the stability limit of state FT. The F/FT interface still propagates into state F, but, since the FT state is now unstable, the system ultimately returns to the F state. This gives rise to a recovery tail that follows the interface. If the ratio of the diffusion of the activator to the diffusion of the main substrates is significantly larger than 1 (here $d>3$), the propagation of the FT state balances the return to the F state at the level of the interface. Thus, the process goes on and a pulse can propagate without damping in time. If d is smaller, or if the system is too far from the stability limit of the FT state, the return to the stable state dominates and the pulse dies. This explains the domain of excitability observed in the experiments and accounted for by the models.

Despite the good agreement of the extended model results with experimental data, this model still presents some serious limitations. A major drawback of the extended model is the use of effective diffusion coefficients which neglects the ionic interactions. The main effect of such interactions is more likely to give different effective diffusion coefficients in the flow state and in the thermodynamic state. As a result, this should change the position of the front and the exact limits of the oscillatory and excitability domains, but we believe that our main conclusions should hold. From an experimental point of view, a severe limitation is the control of parameter uniformity along the annular gel/CSTR boundary which makes the front oscillations to appear in the form of traveling waves. Finally, it has been recently found experimentally that the kinetic mechanisms summarized by Eq. (4) breaks down when the concentration of chlorite or tetrathionate are significantly increased [38].

Beyond these first experimental observations, one can expect to control the front motion by a continuous change of the geometrical control parameter l. Experiments along these lines are presently in progress both numerically and experimentally.

ACKNOWLEDGMENTS

We thank P. Borckmans, G. Dewel, K. Benyaich, and A. De Wit for discussions. This work was supported by the Fundación Antorchas, the C.N.R.S., and a France-Argentina Grant No. ECOS-SCyT.

[1] *Oscillations and Travelling Waves in Chemical Systems*, edited by R. J. Field and M. Burger (Wiley, New York, 1985).
[2] *Chemical Patterns and Waves*, edited by R. Kapral and K. Showalter (Klüwer, Amsterdam, 1995).
[3] I. R. Epstein and J. A. Pojman, *An Introduction to Nonlinear Chemical Dynamics* (Oxford University Press, New York, 1998).
[4] P. Blanchedeau, J. Boissonade, and P. De Kepper, Physica D **147**, 283 (2000).
[5] This does not preclude complex dynamics induced by the diffusive coupling like phase instabilities.
[6] A. Mikhailov, *Foundations of Synergetics I. Distributed Active Systems* (Springer, Berlin, 1994).
[7] V. Castets, E. Dulos, J. Boissonade, and P. De Kepper, Phys. Rev. Lett. **64**, 2953 (1990).
[8] P. De Kepper, V. Castets, E. Dulos, and J. Boissonade, Physica D **49**, 161 (1991).
[9] Q. Ouyang and H.L. Swinney, Nature (London) **352**, 610 (1991).
[10] K.J. Lee, W.D. McCormick, J.E. Pearson, H.L. Swinney, Nature (London) **369**, 215 (1994).
[11] K.J. Lee, D. McCormick, Q. Ouyang, and H. Swinney, Science **261**, 192 (1993).
[12] Á. Tóth, I. Lagzi, and D. Horváth, J. Phys. Chem. **100**, 14 837 (1996).
[13] D. Horváth and Á. Tóth, J. Chem. Phys. **108**, 1447 (1998).
[14] M. Fuentes, M.N. Kuperman, and P. De Kepper, J. Phys. Chem. **105**, 6769 (2001).
[15] I. Lengyel and I.R. Epstein, Science **251**, 650 (1990).
[16] J.E. Pearson and W.J. Bruno, Chaos **2**, 513 (1992).
[17] J. Boissonade, E. Dulos, F. Gauffre, M. Kuperman, and P. De Kepper, Faraday Discuss. **120**, 353 (2001).
[18] P. Gray and S. Scott, *Chemical Oscillations and Instabilities*

(Clarendon Press, Oxford, 1990).
[19] J. Boissonade, in *Dynamics and Stochastic Processes,* edited by R. Lima, L. Streit, and R. Vilela Mendes (Springer, Berlin, 1990), P. 76.
[20] Q. Ouyang, V. Castets, J. Boissonade, J.C. Roux, P. De Kepper, and H.L. Swinney, J. Chem. Phys. **95**, 351 (1991).
[21] P. Blanchedeau and J. Boissonade, Phys. Rev. Lett. **81**, 5007 (1998).
[22] P. Blanchedeau, Ph.D. thesis, Bordeaux, 2000.
[23] I. Nagypal and I.R. Epstein, J. Phys. Chem. **90**, 6285 (1986).
[24] Á. Tóth, D. Horváth, and A. Siska, J. Chem. Soc., Faraday Trans. **93**, 73 (1997).
[25] E. M. Cussler, *Diffusion: Mass Transfer in Fluid Systems* (Cambridge University Press, Cambridge, 1997).
[26] D. Sníta and M. Marek, Physica D **75**, 521 (1994).
[27] K. Benyaich, G. Dewel, and P. Borckmans (unpublished).
[28] D. N. Hague, *Fast Reactions* (Wiley, New York, 1971).
[29] J. A. Dean, *Analytical Chemistry Handbook* (McGraw Hill, New York, 1995).
[30] P. Kaps and P. Rentrop, Numer. Math. **33**, 55 (1979).
[31] P. Deuflhard, SIAM Rev. **27**, 505 (1985).
[32] A.R. Gourlay, J. Inst. Math. Appl. **6**, 375 (1970); A.R. Gourlay and G.R. McGuire, *ibid.* **7**, 216 (1971).
[33] V. Dufiet and J. Boissonade, Physica A **188**, 158 (1992).
[34] J. Boissonade and P. De Kepper, J. Phys. Chem. **84**, 580 (1980).
[35] Z. Noszticzius, W. Horsthemke, W.D. McCormick, H.L. Swinney, and W.Y. Tam, Nature (London) **329**, 619 (1987).
[36] E. Dulos, J. Boissonade, and P. De Kepper, Physica A **188**, 120 (1992).
[37] As usual, this is a first approximation of the stability limits topology. The vicinity of the ''crossing point'' can exhibit more complexity like in Fig. 4(b).
[38] I. Szalaí (private communication).